NASA Technical Memorandum 89900

Hub Flexibility Effects on Propfan Vibration

Michael A. Ernst and Charles Lawrence
Lewis Research Center
Cleveland, Ohio

July 1987

NASA

HUB FLEXIBILITY EFFECTS ON PROPFAN VIBRATION

Michael A. Ernst and Charles Lawrence
National Aeronautics and Space Administration
Lewis Research Center
Cleveland, Ohio 44135

E-3596

SUMMARY

The significance of hub flexibility in the nonlinear static and dynamic analyses of Advanced Turboprop blades is assessed. The blade chosen for this study is the 0.175 scale model of the GE-A7-B4 Unducted Fan blade. A procedure for coupling the effective hub stiffness matrix to an MSC/NASTRAN finite element model is defined and verified. A series of nonlinear static and dynamic analyses are conducted on the blade for both rigid and flexible hub configurations. Results indicate that hub flexibility is significant in the nonlinear static and dynamic analyses of the GE-A7-B4. In order to insure accuracy in analyses of other blades, hub flexibility should always be considered.

INTRODUCTION

Because of the potential for very high propulsive efficiency at cruise speeds up to Mach 0.8, advanced forms of the propeller, called propfans, are being seriously considered for aircraft propulsion. To obtain maximum aerodynamic and acoustic performance, the trend in advanced high speed propeller design has been toward thin, swept blades of complicated structural design (fig. 1). A research program to establish the required technology for successful design of propfans is in progress at the NASA Lewis Research Center (refs. 1 and 2).

Part of this effort is to understand and predict the structural and dynamic behavior of these blades. Normally the MSC or COSMIC NASTRAN finite element computer programs are used to calculate in-vacuum steady state displacements (refs. 3 and 4).

To date, most analyses have assumed that the blades are rigidly attached at their base (fig. 2). This simplification makes blade modeling easier, but does not allow for the effect of hub flexibility to be included in the analysis. The purpose of this study is to determine the effect of hub flexibility on propfan steady state displacement, frequencies, and mode shapes.

The effect of hub flexibility is evaluated by performing steady state displacement and frequency analyses on the GE-A7-B4 Unducted Fan (UDF) blade. Selection of this blade is based on the availability of an effective hub stiffness; characterized by a 6 by 6 stiffness matrix corresponding to the 6 degrees of freedom of the hub attachment point. Unfortunately, a finite element model of the hub is not available. To incorporate this effective hub stiffness into the NASTRAN model, a procedure is developed for coupling a symmetric stiffness matrix to a NASTRAN finite element model. Verification of this procedure, and application to the GE-A7-B4 UDF blade, is presented.

PROCEDURE

This section discusses the coupling procedure for connecting the propfan blade to the effective hub stiffness matrix using the capabilities on NASTRAN. Once this procedure has been implemented, the coupled blade/hub NASTRAN model can be used for both the large displacement (solution 64) and the normal modes (solution 63) analyses (ref. 5). The coupling procedure entails, (1) defining a grid point at the blade to hub attachment location (fig. 3), (2) connecting the grid point defined in 1 to the blade finite element model, and (3) connecting the grid point to the effective hub stiffness matrix.

Either an existing grid point or a newly created grid point may be used for defining the hub attachment location. If an existing grid point coincides with the attachment location, then a new grid point is not required. Otherwise, a new grid point must be created. In figure 3, a new grid point was created because none of the existing grid points coincided with the hub attachment location.

After the grid point is defined, it is attached to its adjacent grid points by rigid bar elements (see ref. 5 for a description of RBAR elements). In the figure, four rigid bar elements are shown which connect the new grid point to four existing grid points on the blade's finite element model. The effect of using the rigid elements is to constrain the new, and four adjacent, grid points to displace as a rigid body. This causes a small region of the finite element mesh to be overly stiff. Since only a small region is constrained, the overall characteristics of the blade will not be affected.

The effective hub stiffness matrix is incorporated into the blade model by using NASTRAN spring elements (CELAS2 cards). Normally CELAS2 cards (fig. 4) are used to connect the degrees of freedom of two unique grid points. For this application, the spring elements are used to specify the coefficients of the effective hub stiffness matrix. This utilization involves connecting springs from the attachment grid point to ground, and using spring elements to specify the coupling between the degrees of freedom at the attachment grid point. The CELAS2 spring elements are used for this application because the NASTRAN large displacement solution sequence (solution 64), unlike some of the other solution sequences, does not permit the direct input of a stiffness matrix.

Twenty one CELAS2 cards are needed to specify the 36 elements of the 6 by 6 effective hub stiffness matrix. Six CELAS2 cards are used for connecting the attachment grid point to ground in the direction of each of the six global degrees of freedom ($u_x, u_y, u_z, \theta_x, \theta_y, \theta_z$). The rest of the CELAS2 cards (15 of them) are used for specifying the cross coupling between the degrees of freedom at the attachment grid point.

The stiffness coefficients for the six grounded terms are computed by summing all of the coefficients in each row of the effective hub stiffness matrix. Each stiffness coefficient is defined by;

$$k_i = \sum_{j=i}^{6} K_{hub\ ij} \quad (i = 1,6)$$

The fifteen springs used to couple the degrees of freedom at the attachment grid point are defined by;

$$k_{ij} = -K_{hub\ ij}$$

where only the off-diagonal coefficients above the diagonal of the hub stiffness matrix are used. The coupling between the degrees of freedom at the attachment grid point is specified by inputing each of the k_{ij} th stiffnesses into field three of the CELAS2 cards. The location of the coupling is specified by inputing the i^{th} and j^{th} degree of freedom numbers into fields five and seven, respectively. The attachment grid point identification is specified in both fields four and six of the CELAS2 card.

As an example, assume that it is desired to connect the stiffness matrix shown in figure 5(a) to an attachment grid point "G1". (A 2 by 2 stiffness matrix is shown for simplicity. In an actual application the stiffness matrix will probably be 6 by 6.) The first row (i = 1) of the stiffness matrix is summed (300+ (-100)) and the resulting spring value is specified in field three of the CELAS2 card (fig. 5(b)). A "1" is specified in field five, and the attachment grid point identification is specified in field four. Fields six and seven are left blank indicating that the spring is connected to ground.

Next, the second row (i = 2) is summed and the result is specified in the second CELAS2 card (fig. 5(c)). This spring is also connected to ground. Only two grounded springs are required for this example because the stiffness matrix is only 2 by 2. As previously mentioned, a 6 by 6 matrix requires the specification of 6 grounded springs.

The coupling spring ($k_{ij} = -(-100)$) is specified in the CELAS2 card shown in figure 5(d). This spring is used to couple the first and second degrees of freedom. The NASTRAN program will automatically insert a 100 into the first and second diagonal elements of the matrix, and a -100 into the off-diagonal locations. Note that the 100 inserted on the diagonal is added to the values that were previously specified via the springs in figures 5(b) and (c). For this example, only one coupling spring is required; where as for a 6 by 6 matrix, 15 coupling springs would be needed.

VERIFICATION

The proceeding procedure for connecting the blade to the hub was verified with a flat plate consisting of seven brick elements (fig. 6). The model is cantilevered, has a length of 14, a width of 2, and depth of 0.4. The brick elements are limited to three translational degrees of freedom at each grid point. All seven brick elements have equal size, and material properties.

Verification of the defined procedure consists of the following:

(1) A dynamic analysis of the full flat plate model described above. Results of this analysis will act as a control for the following analyses.

(2) A dynamic analysis of the reduced flat plate model shown in figure 7. This model is generated by substituting element seven with its effective mass and stiffness matrices. These matrices are attached to grid point 33 and then point 33 is attached to the base with rigid elements. The effective mass matrix is applied to grid point 33 with CONM1 cards.

(3) A repeat of the analysis in the above omitting the effective mass matrix.

The effective mass and stiffness matrices are derived from element seven's property matrices using static condensation (see OMIT card, ref. 5).

Table I presents the first bending, torsion, and edgewise bending frequencies recorded for analyses 1 to 3. For the three analyses conducted, both bending frequencies compare favorably with, at most, a 2.5 percent frequency shift between analyses 1 and 3. Also, it is apparent that the significance of the effective mass matrix is negligible with at most a 0.03 percent first edgewise bending frequency shift between analyses 2 and 3. However, added torsional stiffness exists in the reduced flat plate model, resulting in a 14.3 percent first torsional frequency shift between analyses 1 and 3. As mentioned in the proceeding section, this added torsional stiffness in analyses 2 and 3 is due to the constraints applied by the rigid elements. These constraints require that the bottom face of element 6 remains quadrilateral, when in fact it warps in the torsional mode. Because of the simplified model used for verification of procedure, the effects of added torsional stiffness are more dramatic. In propfan analysis, it is safe to assume that the added torsional stiffness due to constraints will be negligible because the rigid elements only constrain a small portion of the blade's base with respect to the size of the model, and the number of elements used (fig. 3).

APPLICATION

The blade chosen to assess hub flexibility is the 0.175 scale model of the GE-A7-B4. The finite element model of this blade, along with the effective stiffness matrix characterizing hub flexibility, has been provided by the General Electric Company (fig. 8). To assess the effect of hub flexibility, a series of large displacement and dynamic analyses were performed at various rotational speeds using MSC/NASTRAN's solution sequence 64 and 63, respectively.

Figure 9 presents the additional cards included in the bulk data deck of GE-A7-B4's finite element model in order to account for hub flexibility. The GRID card defines the massless, 6 degrees of freedom grid point, 757, where the hub flexibility matrix is to be applied (fig. 10). The RBAR cards constrain the degrees of freedom of grid point 734, 735, 742, and 743 to the degrees of freedom of grid point 757. And the CELAS2 cards add the stiffness influence coefficients, defined by the effective hub stiffness matrix, directly into the global stiffness matrix of the finite element model with spring constants defined by the procedure section of this paper.

Results of the analyses are presented in tables II and III, and figures 11 and 12. Figure 11 presents the magnitude of leading edge tip displacements versus rotational speed, for both rigid and flexible hubs. At low rpm, the

flexible hub has little effect on the static displacement of the GE-A7-B4. However, at rpm's greater than 4000, the influence of the flexible hub becomes notable. Figure 12 presents the first bending, second bending, first torsional, and third bending eigenvalues for the GE-A7-B4 at various rpm's, in both rigid hub and flexible hub configurations. While the first bending and first torsional frequencies seem to be unaffected by the flexible hub, there is an appreciable discrepancy between the flexible hub and the rigid hub configurations concerning the second bending and third bending frequencies. Also shown in figure 12 is an edgewise mode that is being picked up in the flexible hub configuration. The frequency of this mode lies between the second bending and first torsional modes. The first edgewise mode was not seen for the rigid hub configuration in the lower frequency range. Figure 13 presents nodal line plots for the mode shapes discussed above.

SUMMARY AND CONCLUSION

The GE-A7-B4 UDF blade was chosen to assess the effects of hub flexibility on propfan blade vibrations. This blade was chosen due to the availability of a 6 by 6 nodal stiffness matrix characterizing hub flexibility. A finite element model of the hub was not available.

In order to assess the effects of hub flexibility, a series of large displacement and dynamic analyses needed to be performed at various rpm's using MSC/NASTRAN's solution sequences 64 and 63, respectively. While most MSC/NASTRAN solution sequences allow for the modification of the global stiffness matrix with stiffness coefficients, there was no direct method to apply the hub stiffness matrix to the blade's finite element model in a solution 64 large displacement analysis. A procedure was therefore developed, and verified, allowing for the coupling between a symmetric stiffness matrix and a NASTRAN finite element model in a solution 64 large displacement analysis. Although this procedure was demonstrated using an analytically derived effective hub stiffness, it is equally applicable for an experimentally obtained hub stiffness.

The effect of hub flexibility on steady state displacement and frequencies has been shown to be significant for the GE-A7-B4 Unducted Fan blade. A drop in the second bending, third bending, and first edgewise modal frequencies may have a significant impact on any aeroelastic analysis conducted on the blade.

Overall, in order to insure accuracy in analyses of other propfan blades, hub flexibility should always be considered. If hub flexibility effects are not assessed, the accuracy of the results will be questionable.

REFERENCES

1. Mikkelson, D.C.; Mitchell, G.A.; and Bober, L.J.: Summary of Recent NASA Propeller Research. NASA TM-83733, 1984.

2. Strack, W.C., et al.: Technology and Benefits of Aircraft Counter Rotation Propellers. NASA TM-82983, 1981.

3. McGee, O.G.: Finite Element Analysis of Flexible Rotating Blades. NASA TM-89906, 1987.

4. Lawrence, C., et al.: A NASTRAN Primer for the Analysis of Rotating Flexible Blades. NASA TM-89861, 1987.

5. McCormick, C.W., ed.: MSC/NASTRAN User's Manual, Vol. I, MacNeal-Schwendler, 1983.

TABLE I. - RESULTS OF PROCEDURE VERIFICATION

Model / Mode	Frequencies, Hz		
	Full flat plate	Reduced flat plate, 6 by 6 nodal mass and stiffness matrices replacing element 7	Reduced flat plate, 6 by 6 nodal stiffness matrix replacing element 7
First bending	64.7	66.3	66.3
First torsion	496.0	566.9	567.0
First edgewise bending	316.9	322.5	322.6

TABLE II. - GE-A7-B4 LEADING EDGE TIP DISPLACEMENTS: RIGID HUB VERSUS FLEXIBLE HUB (PERCENT SPAN LENGTH)

rpm	Rigid hub	Flexible hub
3000	0.1878	0.1931
4000	.2922	.3053
5000	.3923	.4205
6000	.4803	.5348
7000	.5527	.6496
8000	.6104	.7682

TABLE III. - GE-A7-B4 MODAL FREQUENCIES (Hz)

rpm	Mode	Rigid hub	Flexible hub
0	1B	198.26	188.45
	2B	577.07	502.77
	1E		675.21
	1T	757.46	748.47
	3B	1215.19	1120.14
2000	1B	206.31	196.18
	2B	582.83	508.03
	1E		678.95
	1T	764.61	754.16
	3B	1220.90	1127.76
3000	1B	215.89	205.35
	2B	589.69	514.32
	1E		683.42
	1T	773.77	761.64
	3B	1227.93	1137.22
4000	1B	228.49	217.40
	2B	598.72	522.62
	1E		689.35
	1T	786.88	772.59
	3B	1237.58	1150.33
5000	1B	243.56	231.78
	2B	609.45	532.51
	1E		696.55
	1T	804.02	787.22
	3B	1249.67	1166.88
6000	1B	260.54	247.94
	2B	621.44	543.58
	1E		704.86
	1T	825.12	805.55
	3B	1263.99	1186.58
7000	1B	278.86	265.47
	2B	634.26	555.48
	1E		714.21
	1T	849.78	827.44
	3B	1280.25	1209.08
8000	1B	298.38	283.86
	2B	647.80	567.81
	1E		724.46
	1T	877.88	852.37
	3B	1298.45	1233.80

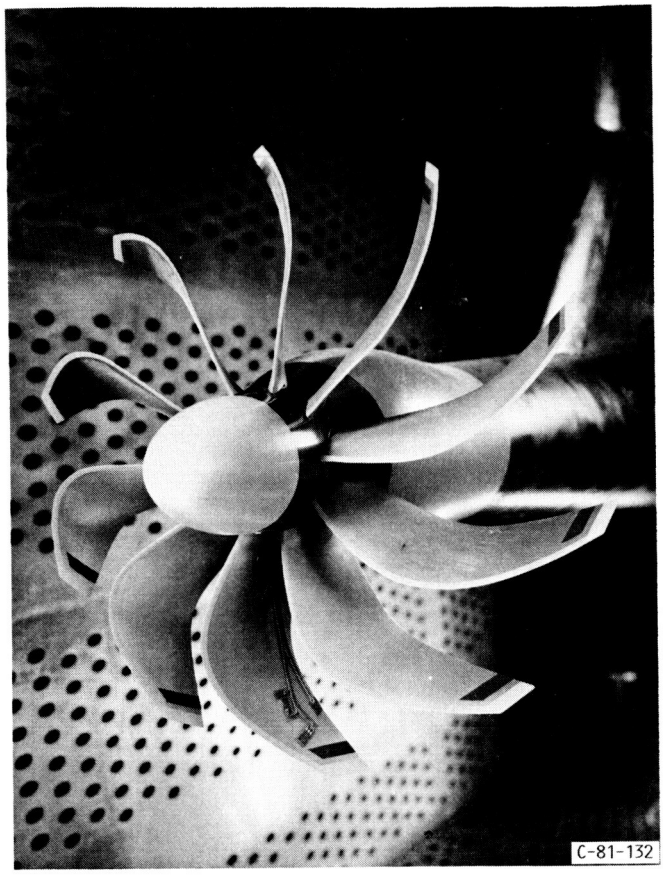

FIGURE 1. - PROPFAN.

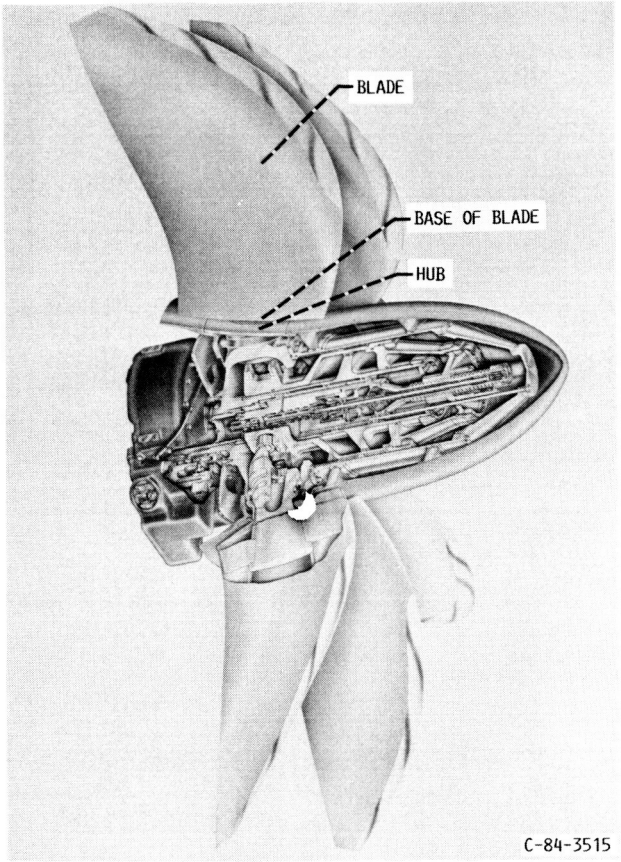

FIGURE 2. - PROPFAN ASSEMBLY.

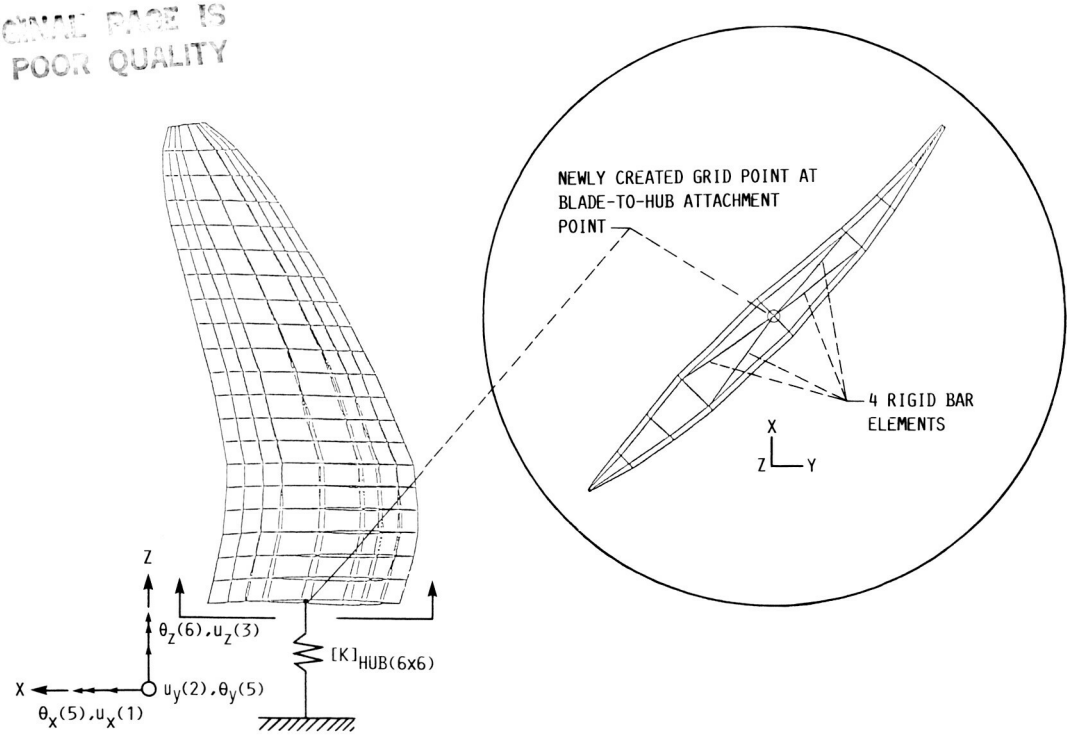

FIGURE 3. - BLADE-TO-HUB ATTACHMENT POINT.

INPUT DATA CARD CELAS2 SCALAR SPRING PROPERTY AND CONNECTION

DESCRIPTION: DEFINES A SCALAR SPRING ELEMENT OF THE STRUCTURAL MODEL WITHOUT REFERENCE TO A PROPERTY CARD.

FORMAT

1	2	3	4	5	6	7	8	9	10
CELAS2	EID	K	G1	C1	G2	C2	GE	S	

FIELD	CONTENTS
EID	UNIQUE ELEMENT IDENTIFICATION NUMBER (INTEGER >0)
K	THE VALUE OF THE SCALAR SPRING (REAL)
G1,G2	GEOMETRIC GRID POINT IDENTIFICATION NUMBER (INTEGER ≥ 0)
C1,C2	COMPONENT NUMBER ($6 \geq$ INTEGER ≥ 0)
GE	DAMPING COEFFICIENT (REAL)
S	STRESS COEFFICIENT (REAL)

FIGURE 4. - CELAS2 CARD.

$$\begin{array}{c} \\ 1 \\ 2 \end{array} \begin{array}{c} \begin{array}{cc} 1 & 2 \end{array} \\ \begin{bmatrix} 300 & -100 \\ -100 & 250 \end{bmatrix} \end{array} \qquad \text{(a)}$$

EFFECTIVE STIFFNESS MATRIX (2 DOF)

$$\begin{bmatrix} 200 & --- \\ --- & --- \end{bmatrix} \qquad \text{(b)}$$

CELAS2,"EID1",200,"G1",1

$$\begin{bmatrix} 200 & --- \\ --- & 150 \end{bmatrix} \qquad \text{(c)}$$

CELAS2,"EID2",150,"G1",2

$$\begin{bmatrix} (200 + 100) & -100 \\ -100 & (150 + 100) \end{bmatrix} \qquad \text{(d)}$$

CELAS2,"EID3",100,"G1",1,"G1",2

FIGURE 5. - CONNECTING A 2 DOF EFFECTIVE STIFFNESS MATRIX TO GRID POINT "G1".

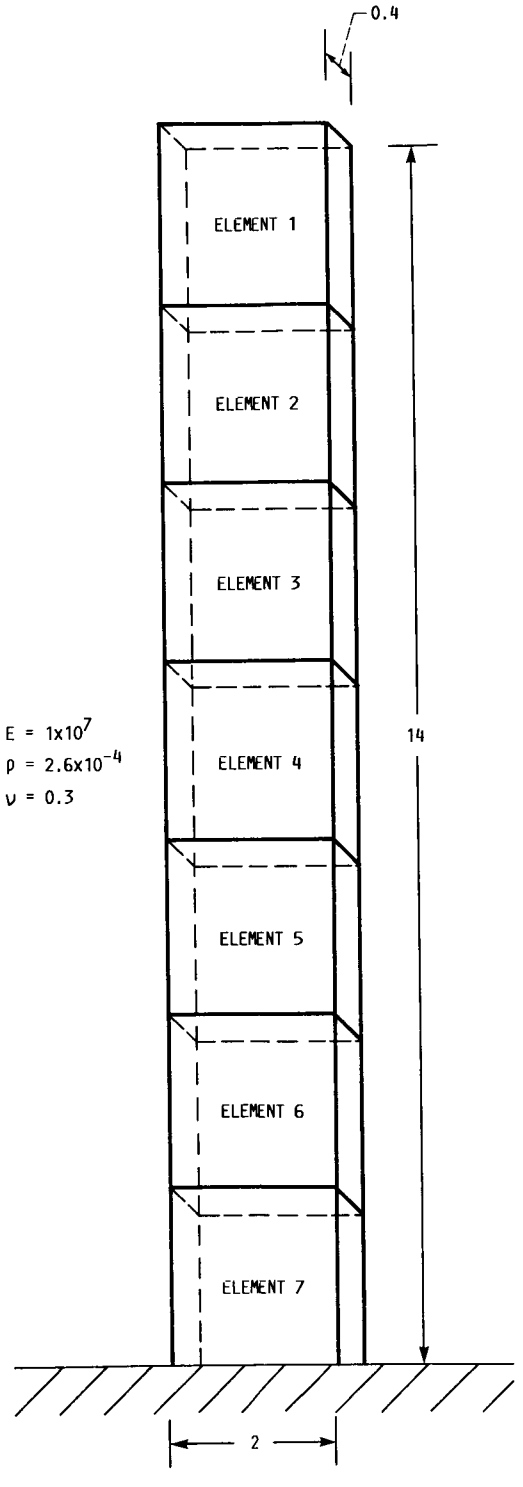

FIGURE 6. - FLAT PLATE MODEL.

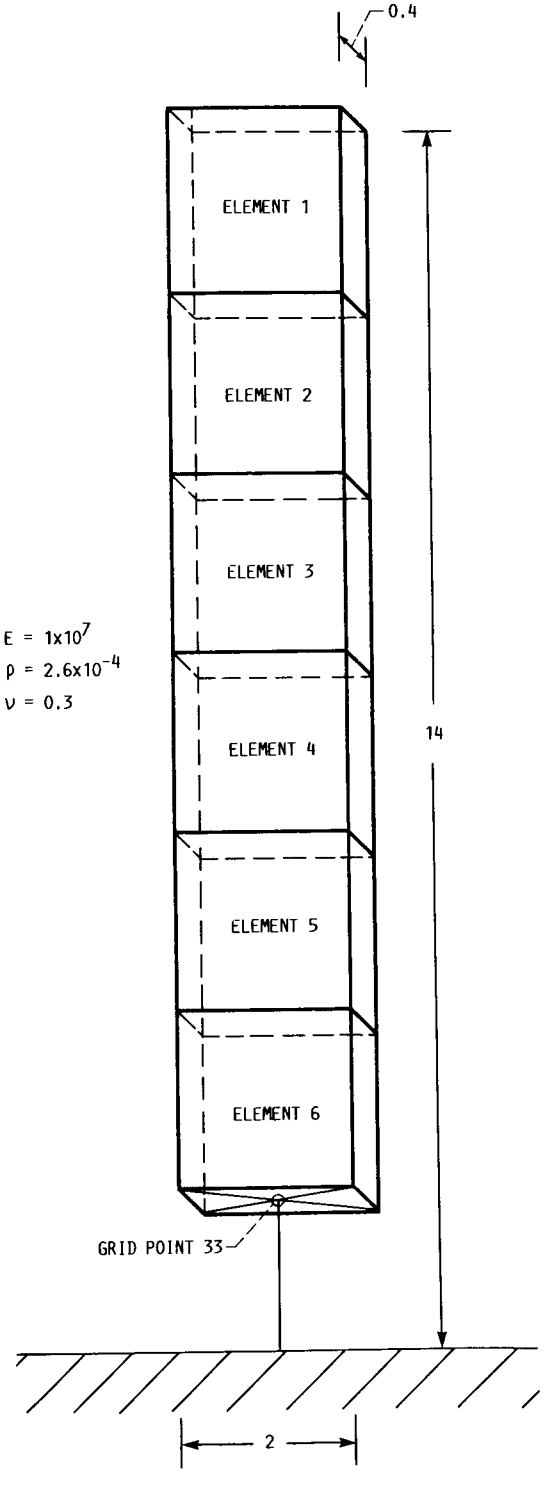

FIGURE 7. - REDUCED FLAT PLATE MODEL.

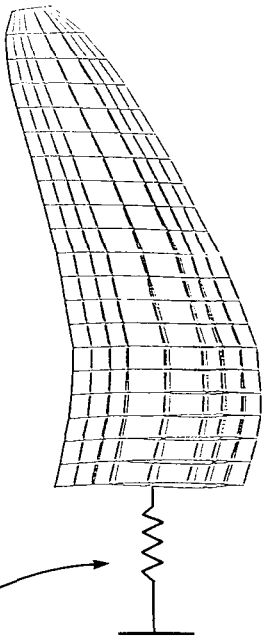

$$[K]_{HUB} = \begin{bmatrix} 1.958\ E5 & 5.500\ E1 & 7.672\ E3 & 1.500\ E1 & 1.253\ E5 & 2.940\ E2 \\ 5.500\ E1 & 7.472\ E5 & -2.800\ E2 & 1.663\ E5 & 6.700\ E1 & -4.707\ E4 \\ 7.672\ E3 & -2.800\ E2 & 2.478\ E4 & -4.900\ E1 & 7.935\ E3 & 5.330\ E2 \\ 1.500\ E1 & 1.663\ E5 & -4.900\ E1 & 7.085\ E4 & -4.200\ E2 & -1.316\ E4 \\ 1.253\ E5 & 6.700\ E1 & 7.935\ E3 & -4.200\ E2 & 1.095\ E5 & 6.990\ E2 \\ 2.940\ E2 & -4.707\ E4 & 5.330\ E2 & -1.316\ E4 & 6.990\ E2 & 6.115\ E5 \end{bmatrix}$$

FIGURE 8. - FINITE ELEMENT MODEL OF GE-A7-B4 AND EFFECTIVE HUB STIFFNESS MATRIX.

```
GRID      757          -0.0102  0.0578  4.9572
RBAR      100    757   742   123456                  123
RBAR      200    757   743   123456                  123
RBAR      300    757   735   123456                  123
RBAR      400    757   734   123456                  123
CELAS2     11 329209.   757     1
CELAS2     22 866345.   757     2
CELAS2     33  40591.   757     3
CELAS2     44 223558.   757     4
CELAS2     55 243175.   757     5
CELAS2     66 552796.   757     6
CELAS2     12    -55.   757     1     757     2
CELAS2     13  -7672.   757     1     757     3
CELAS2     14    -15.   757     1     757     4
CELAS2     15-125348.   757     1     757     5
CELAS2     16   -294.   757     1     757     6
CELAS2     23    280.   757     2     757     3
CELAS2     24-166324.   757     2     757     4
CELAS2     25     67.   757     2     757     5
CELAS2     26  47071.   757     2     757     6
CELAS2     34     49.   757     3     757     4
CELAS2     35  -7935.   757     3     757     5
CELAS2     36   -533.   757     3     757     6
CELAS2     45    420.   757     4     757     5
CELAS2     46  13163.   757     4     757     6
CELAS2     56   -699.   757     5     757     6
```

FIGURE 9. - MSC/NASTRAN BULK DATA DECK CARDS ACCOUNTING FOR HUB FLEXIBILITY.

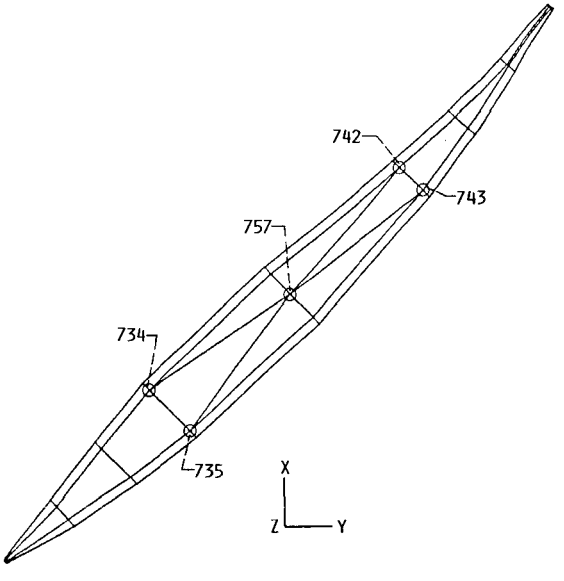

FIGURE 10. - BLADE ROOT.

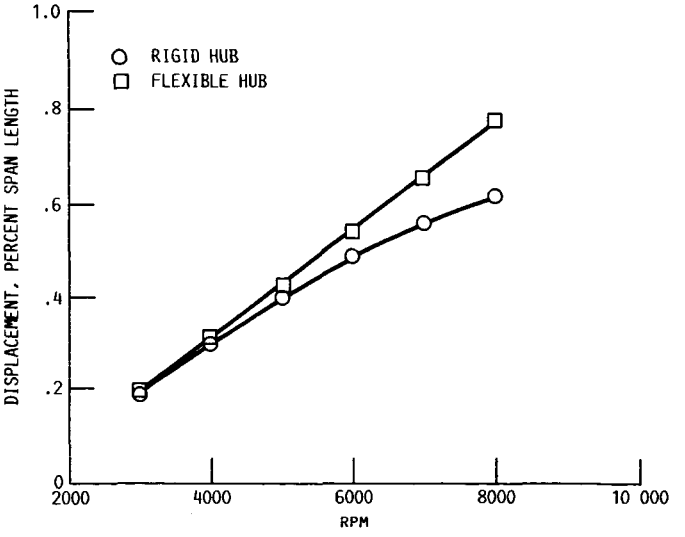

FIGURE 11. - GE-A7-B4 LEADING EDGE TIP DISPLACEMENTS. RIGID HUB VERSUS FLEXIBLE HUB.

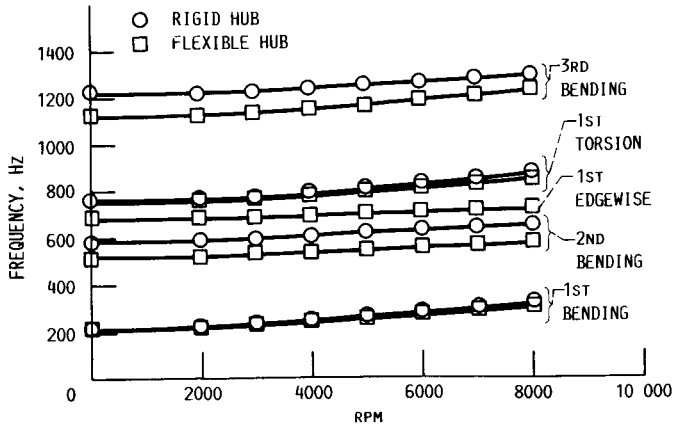

FIGURE 12. - GE-A7-B4 MODAL FREQUENCIES. RIGID HUB VERSUS FLEXIBLE HUB.

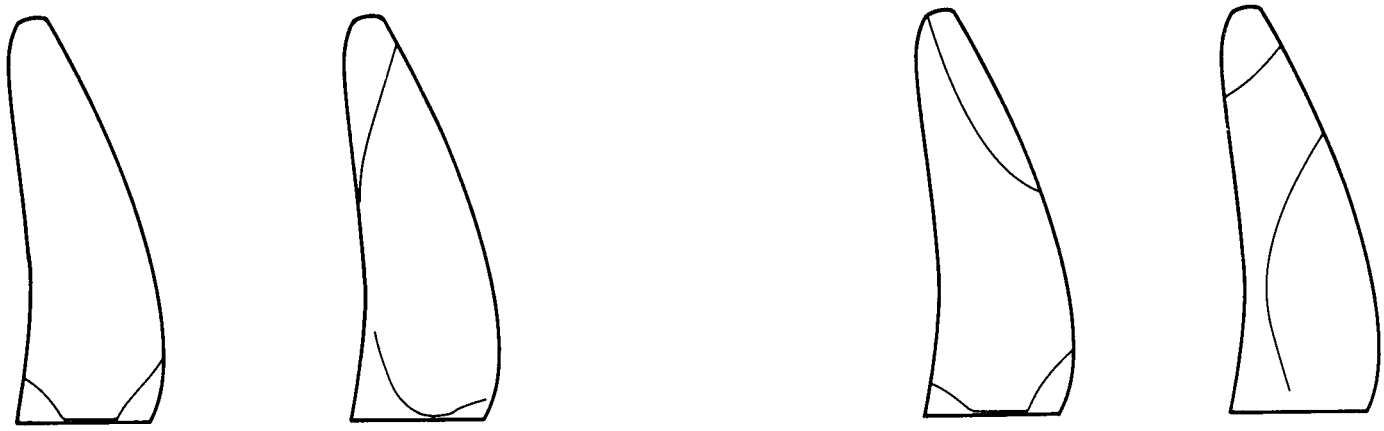

RIGID HUB

1B 2B 1E 1T 3B

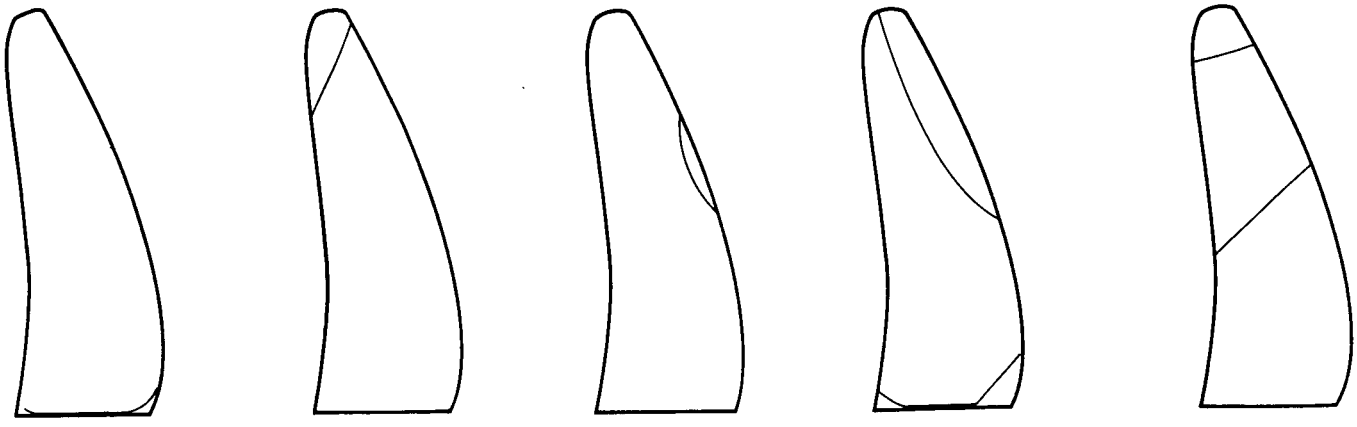

FLEXIBLE HUB

FIGURE 13. - GE-A7-B4 NODAL LINE PLOTS.

NASA
National Aeronautics and Space Administration

Report Documentation Page

1. Report No.	2. Government Accession No.	3. Recipient's Catalog No.
NASA TM-89900		

4. Title and Subtitle

Hub Flexibility Effects on Propfan Vibration

5. Report Date

July 1987

6. Performing Organization Code

505-63-11

7. Author(s)

Michael A. Ernst and Charles Lawrence

8. Performing Organization Report No.

E-3596

10. Work Unit No.

9. Performing Organization Name and Address

National Aeronautics and Space Administration
Lewis Research Center
Cleveland, Ohio 44135

11. Contract or Grant No.

13. Type of Report and Period Covered

Technical Memorandum

12. Sponsoring Agency Name and Address

National Aeronautics and Space Administration
Washington, D.C. 20546

14. Sponsoring Agency Code

15. Supplementary Notes

16. Abstract

The significance of hub flexibility in the nonlinear static and dynamic analyses of Advanced Turboprop blades is assessed. The blade chosen for this study is the 0.175 scale model of the GE-A7-B4 Unducted Fan blade. A procedure for coupling the effective hub stiffness matrix to an MSC/NASTRAN finite element model is defined and verified. A series of nonlinear static and dynamic analyses are conducted on the blade for both rigid and flexible hub configurations. Results indicate that hub flexibility is significant in the nonlinear static and dynamic analyses of the GE-A7-B4. In order to insure accuracy in analyses of other blades, hub flexibility should always be considered.

17. Key Words (Suggested by Author(s))	18. Distribution Statement
Advanced turboprop Finite element analysis NASTRAN	Unclassified - unlimited STAR Category 39

19. Security Classif. (of this report)	20. Security Classif. (of this page)	21. No of pages	22. Price*
Unclassified	Unclassified	15	A02

*For sale by the National Technical Information Service, Springfield, Virginia 22161